Long Discontinuous Fiber Composite Structure - Forming and Structural Mechanics[1*]

R. B. Pipes, M. H. Santare, B. J. O'Toole, A. J. Beaussart, D. C. DeHeer
Department of Mechanical Engineering and the Center for Composite Materials University of Delaware
R. K. Okine
E. I. du Pont de Nemours and Co., Inc.

Abstract

Cost effective composite structure has motivated the investigation of several new approaches to develop composite structure from innovative material forms. Among the promising new approaches is the conversion of planar sheet to components of complex curvature through sheet forming or stretch forming. In both cases the potential for material stretch in the fiber direction appears to offer a clear advantage in formability over continuous fiber systems. In the present study the authors have established a framework which allows the simulation of the anisotropic mechanisms of deformation of long discontinuous fiber laminates wherein the matrix phase is a viscous fluid.

The initial study focuses upon the establishment of micromechanics models for prediction of the effective anisotropic viscosities of the oriented fiber assembly in a viscous matrix. Next, the developed constitutive relation is employed through an analogy with incompressible elasticity to exercise the finite-element technique for determination of local fiber orientation and laminate thickness after forming. Results are presented for the stretch bending of a curved beam from an arbitrary composite laminate and the bulging of a clamped sheet.

Structural analyses are conducted to determine the effect of microstructure on the performance of curved beams manufactured from long discontinuous fiber composites. For the purposes of this study, several curved beams with ideal and non-ideal microstructures are compared for response under pure bending. Material parameters are determined from a separate microstructural analysis.

Micromechanics of Forming

Models for prediction of the effective anisotropic viscosities of an oriented assembly of discontinuous fibers (Figure 1) suspended in a power-law, viscous fluid with finite yield stress have been developed as summarized in Table 1. The present theory for the axial elongational viscosity is compared to a relation for non-dilute suspensions developed by Batchelor [1] in Figure 2. The Batchelor predictions are shown to be restricted to relatively small fiber volume fractions while the present theory was shown to be valid for volume fractions above 0.196. The models for both shearing viscosities are shown to satisfy the bonds at zero and maximum fiber volume fraction.

Results presented in Table 1 show the influence of power-law exponent upon each viscosity term as a function of strain rate. For finite yield stress of the matrix fluid, the effective yield stress of the assembly was determined for the two shearing and two elongational modes of deformation. Only in

1* NASA Contract NAS1-18758 Program Monitor: Dawn Jegley

the case of longitudinal elongational mode did the effective yield stress differ from the matrix yield stress.

Fiber overlap length and geometry have been evaluated for their influence upon the effective elongational viscosity of an oriented fiber array. The results indicate that the developed relations are equivalent for both symmetric and asymmetric overlap geometries as shown in Figure 3. For variation in fiber length and overlap length within the assembly, an integral representation has developed and normalized frequency functions for fiber length and overlap length of zeroth and first order have been evaluated assuming independence of the two frequency distributions. Effective viscosity calculated for typical fiber length data shown in Figure 4 reveal that small percentages in long fibers can have a disproportionately large influence upon results as shown in Figure 5.

Two laminate theories have been developed for the prediction of the effective anisotropic viscosities of oriented discontinuous fiber assemblies suspended in a Newtonian fluid. The first theory is an analogy with classical laminate theory for elastic systems wherein the laminae are constrained to exhibit identical states of strain rate. Results presented in Table 2 for the pseudo laminate theory reveal that the highly anisotropic nature of the oriented fiber lamina is transferred to the laminate behavior. Indeed, laminates were constructed wherein the effective elongational viscosities are several orders of magnitude greater than the effective in-plane shearing viscosity, while other laminates were shown to possess effective in-plane shearing viscosity which greatly exceeded both effective elongational viscosities. The second theory allows individual lamina to be unconstrained by one another. In all the cases presented the values of effective viscosities of the laminates were greater for the constrained condition than for the unconstrained condition as shown in Table 3.

The influence of fiber orientation on elongational viscosity $\eta'_{11}(\theta)$ for the highly anisotropic lamina is shown in Figure 6 as a function of fiber aspect ratio (L/D). These results show that the viscosity of the lamina diminishes by three orders of magnitude for $\theta=1°$ and L/D = 10,000. In Figure 7 the expected value of viscosity $\langle\eta_{11}\rangle$ for disoriented fibers is shown. Here the probability of fibers at orientation, θ is equal between $+\theta_1$ and $-\theta_1$. Again note that the apparent viscosity is a strong function of fiber misorientation.

Macromechanics of Forming

Consider the equivalent anisotropic constitutive relationship for the oriented fiber assembly described above in a state of plane stress:

$$\begin{pmatrix} \dot{\varepsilon}_{11} \\ \dot{\varepsilon}_{22} \\ \dot{\varepsilon}_{12} \end{pmatrix} = \begin{pmatrix} \frac{1}{\eta_{11}} & -\frac{1}{2\eta_{11}} & 0 \\ -\frac{1}{2\eta_{11}} & \frac{1}{\eta_{22}} & 0 \\ 0 & 0 & \frac{1}{2\eta_{12}} \end{pmatrix} \begin{pmatrix} \sigma_{11} \\ \sigma_{22} \\ \sigma_{12} \end{pmatrix} \qquad (1)$$

The (3 x 3) matrix in equation 1 can be inverted although the material is incompressible. The reciprocal stress/strain rate relation is

$$\begin{pmatrix} \sigma_{11} \\ \sigma_{22} \\ \sigma_{12} \end{pmatrix} = \begin{pmatrix} C_{11} & C_{12} & 0 \\ C_{12} & C_{22} & 0 \\ 0 & 0 & 2C_{66} \end{pmatrix} \begin{pmatrix} \dot{\varepsilon}_{11} \\ \dot{\varepsilon}_{22} \\ \dot{\varepsilon}_{12} \end{pmatrix} \qquad (2)$$

where

$$C_{11} = \frac{4\,\eta_{11}^2}{4\,\eta_{11} - \eta_{22}} \qquad C_{22} = \frac{4\,\eta_{11}\,\eta_{22}}{4\,\eta_{11} - \eta_{22}}$$

$$C_{12} = \frac{2\,\eta_{11}\,\eta_{22}}{4\,\eta_{11} - \eta_{22}} \qquad C_{66} = \eta_{12} \qquad (3)$$

In the present work we have followed the approach used in finite element analysis for viscoplastic forming of metallic material. Two differences between the case of a viscoplastic metal and a reinforced thermoplastic must be noted. First, the constitutive equation is linear for the composite material considered here, while a non-linear model is followed for metal forming to account for the high strain-rate dependence. Each step of the solution scheme is solved in one iteration for the composite material. The linear model is obviously a simplification of the problem. Average values of the anisotropic viscosities must be chosen in the range of values typical for the forming processes considered. The second difference is due to the anisotropy of the composite material. The flow

formulation and the finite-element discretization are perfectly valid for an anisotropic material. However, the fiber orientation change must be taken into account after each stage (time step) of the forming simulation, which corresponds to a small deformation. One can easily imagine that the fiber orientation in a sheet will not keep its initial direction, but will vary locally if the process involves large deformations. The solution scheme for the simulation of the sheet forming of a viscous, anisotropic material is as follows:

- Input: initial geometry and material parameters.
- Simulation:
  1. Solve for the velocity field "V" using the analogy to classical elasticity theory.
  2. Update the geometry by "$V\Delta t$" where "Δt" is an appropriate time step.
  3. Update the local fiber orientation and the sheet thickness.
  4. Change the boundary conditions if new points come into contact with the mold surface.
  5. Repeat the process until pre-determined deformation is reached or until contact with mold is complete.
- Output at each step: components of stress and strain rate, updated geometry, thickness and fiber orientation distribution.

Implementation of the Plane Stress Formulation

One of the advantages of this method is the possibility of using existing finite element codes developed for elasticity to solve viscous creeping flow problems. Consider the case of the off axis tensile test shown in Figure 8 a. Results for deformed shape after 20 time steps are shown in Figure 8 b and corresponding fiber orientation in Figure 8 c. Consider the next the bending of a flat sheet of unidirectional material (Figure 9). The resulting deformed shape and fiber orientation are shown in Figure 9 b. Finally consider the bulging of a flat plate of 45° fiber orientation subjected to a lateral pressure shown in Figure 10. The results offer 20 time steps and after 59 steps are shown in Figures 10 b and 10 c, respectively.

Forming Experiments

Curved C-channel structures have been manufactured from a planar, long discontinuous fiber laminate through a diaphragm forming process. The chosen diaphragm material is a superplastic aluminium alloy 2004. The long, discontinuous fiber laminates consist of a PEKK thermoplastic resin and PAN-based fibers, AS-4, that are approximately 2.2 inches in length.

To insure successful manufacture of the C-channel structure, two molding techniques were employed simultaneously. First, PEI films were placed between the composite and the diaphragm

material to act as a lubricating layer. For added flexibility, the PEI film can be used in joining thermoplastics by means of resistance welding. The second technique was to reduce the composite preform area, thus resulting in less excess material after molding. The size of the composite preform was found to influence the final shape and success of the structure.

The composite was isothermally formed at 390° C and was pressurized at 5 psi/min. (on average) with 5 minute dwells at 20 psi and 150 psi. The maximum pressure of 150 psi was maintained during cooling. Vacuum pressure between the diaphragms was held throughout the process.

The curved C-channel structures were manufactured from 8 ply, unidirectional laminates. Future studies will be performed using various stacking sequences and thicknesses to determine these parameters' effects on microstructure. The resulting components are shown in Figure 11.

Structural Micromechanics

The elastic properties of advanced composite materials depend strongly upon the orientations of the reinforcing components utilized. To better understand the structural performance of discontinuous fiber components the microstructural characteristics of formed parts must be determined. Toward this end, a study was conducted to evaluate two orientation parameters; relative fiber alignment and average fiber orientation.

Ideally, a ply of unformed fibrous composite sheet is unidirectional. However, processing limitations create sheets of the material that are not truly unidirectional. There will be some degree of fiber misalignment in a typical sample of unprocessed material.

During the manufacture of parts with discontinuous fiber material, some microstructural changes occur. The formation of curved components involves the forming of the originally flat material preform over a contoured surface. The fibers in the some portions of the material may tend to align themselves while fibers in other regions may become less aligned during the forming process. The local elastic properties are altered accordingly, producing a material with mechanical characteristics different than those of unformed sheets.

In order to determine the relationship between fiber alignment and mechanical properties, a computer program developed at the University of Delaware's Center for Composite Materials was employed [2]. The Sheet Molding Composites (SMC) program calculates the engineering constants of composite materials from basic input data.

The SMC program utilizes an aggregate model approach that reduces the composite material to a collection of typical reinforcing fiber regions and orientationally averages the properties of these regions. The relative alignment of these regions is described by a value known as Herman's orientation parameter f_p. Completely randomly oriented fibers produce a Herman's orientation of 0, while a value of 1 results from perfectly aligned fibers. In addition to the effective aspect ratio and Herman's orientation, the

program requires the mechanical properties of the fibers and matrix as input. These characteristics include elastic modulus, shear modulus, and Poisson's ratio. Fiber volume fraction of the composite material is also needed.

The parameter f_p is calculated in the following manner. The equation given below defines Herman's orientation as a function of a trigonometric average

$$f_p = 2 \langle \cos^2 \phi \rangle - 1 \tag{4}$$

where

$$\langle \cos^2 \phi \rangle = \int_0^{\frac{\pi}{2}} n(\phi) \cos^2 \phi \, d\phi \tag{5}$$

and ϕ is the orientation of the individual regions. Here $n(\phi)$ is the distribution function that describes the relative number of regions oriented at an angle ϕ with respect to the average fiber orientation. This function can be calculated for a particular sample with a histogram. N is assumed to be the total number of fibers counted and $N(\phi_i)$ is the number of fibers falling within $\phi_i \pm \Delta\phi$ of the average fiber direction. The value $\langle \cos^2 \phi \rangle$ can then be found from the following relation:

$$\langle \cos^2 \phi \rangle = \frac{1}{N} \sum_{i=1}^{N} N(\phi_i) \cos^2 \phi_i. \tag{6}$$

According to the supplier, the fiber volume fraction of the material samples studied was 0.60. In addition, the fiber length for these samples was given to be approximately 2 in. Using an average fiber diameter of 295 μin, an effective aspect ratio of 6780 was calculated.

An example of the estimation of Herman's orientation is summarized here. A micrograph of unprocessed material was analyzed and the histogram depicted in Figure 12 was obtained. A value of 0.997 was subsequently calculated for the Herman's orientation. Two samples of unprocessed sheet were analyzed, with an average Herman's orientation of 0.994. In addition, five samples of material formed into a spherical shell were examined. An average orientation parameter of 0.995 was found. The calculation of mechanical properties by the SMC program utilized the material parameters of PEKK resin and AS-4 carbon fibers. The relationship between relative fiber alignment and several material

properties is shown in Figure 13. The results show that relative fiber orientation has little effect on elastic properties in these unidirectional discontinuous fiber composites before and after processing.

In parts manufactured using a diaphragm forming process, the average fiber axes are not perfectly aligned with structural axes. Consequently the elastic properties of a given part vary depending upon local fiber orientation. It is necessary to determine structural engineering constants from the material properties of the composite and the average reinforcing fiber orientation. The most direct method of performing the transformation makes use of the compliance matrix of the material. The transformation matrix for the properties in the plane of the material is depicted below:

$$\begin{bmatrix} S_{11} \\ S_{22} \\ S_{12} \\ S_{66} \end{bmatrix} = \begin{pmatrix} m^4 & n^4 & 2m^2n^2 & m^2n^2 \\ n^4 & m^4 & 2m^2n^2 & m^2n^2 \\ m^2n^2 & m^2n^2 & m^4 + n^4 & -m^2n^2 \\ 4m^2n^2 & 4m^2n^2 & -8m^2n^2 & (m^2 - n^2)^2 \end{pmatrix} \begin{bmatrix} S_{xx} \\ S_{yy} \\ S_{xy} \\ S_{ss} \end{bmatrix} \qquad (7)$$

Where the 1, 2 subscripts refer to the structural axes (the tangential and radial directions in the case of the curved beam) and the x,y subscripts refer to the material axes (x-being the local average fiber direction). Also $m = \cos \alpha$, $n = \sin \alpha$, and α is the angle between the average fiber axis x and the structural axis 1.

The structural engineering constants may then be determined by the following relations:

$$E_1 = \frac{1}{S_{11}} \qquad E_2 = \frac{1}{S_{22}}$$

$$G_{12} = \frac{1}{S_{66}} \qquad \upsilon_{12} = -\frac{S_{12}}{S_{22}} \qquad (8)$$

A typical curved part was manufactured in a diaphragm forming process as described in the previous section. A microstructural analysis was performed to determine the average fiber orientation at a number of points in the curved beam. Equation (8) was then used to calculate the the local material properties relative to the structural axes for use in a structural performance analysis.

Structural Macromechanics

The following analysis compares the relative performance of curved beams with several different microstructures based on a maximum stress failure criterion. The microstructures are chosen to be

representative of different manufacturing procedures. Efficiency of the structure is determined as the ratio of failure load to weight. No attempt was made to include the cost of manufacture or material.

Material heterogeneity is most prevalent in the web section; therefore analysis is conducted for a rectangular cross-section curved beam which represents the web of an I-beam, channel beam, T-beam, etc. Analysis shows that the principal stresses are in the radial and tangential directions for a beam loaded in pure bending and the maximum tangential stress can be several times greater than the maximum radial stress depending on the geometry. This indicates that the efficiency of a beam can be improved by orienting the majority of the fibers in the maximum load direction. Several beams have been produced by diaphragm sheet forming. Preliminary results show that the fiber orientation along the web of these beams is not quite tangential so that the material properties, relative to the beam coordinates, vary along the length of the beam. Figure 14 compares schematically the microstructures of unidirectional and quasi-isotropic curved beams made from stretching a straight beam and diaphragm forming processes with those made from a process which entails cutting a curved pattern out of a flat panel. Both an elasticity analysis and a finite element analysis are conducted to determine the effect of material heterogeneity on the stresses in the beam.

Elasticity Analysis

The analysis is conducted for a curved beam with heterogeneous material properties loaded in pure bending. Figure 15 shows the geometry of a beam loaded in pure bending where a and b are the inside and outside radii, r and q are the radial and tangential coordinates, M is the applied moment, R is the average beam radius, $R = (a + b)/2$, t is the beam depth and d is the distance from the beams centroidal axis. An important geometric parameter is the average radius to depth ratio, R/t.

The analytical solution is based on an elasticity approach similar to that found in Lekhnitskii [3] with the only difference being that the constitutive relation allows for material property variation in both the radial and tangential directions. The analysis is conducted by expressing the radial, tangential and shear stresses in terms of a stress potential, F. The details of this analysis can be found in [3] but the constitutive relation used here is

$$\varepsilon_{ij} = a_{ik}\,\sigma_{kj}, \tag{9}$$

where

$$a_{ik} = \alpha_{ik}\cos(k\,\theta)\,r^{-n}$$

and a_{ij} are the elements of the compliance matrix, α_{ij} are the homogeneous material property base values of a_{ij}, r is the radius, and n and k are the degrees of heterogeneity in the radial and tangential directions respectively. The sign of n determines whether the beam is stiffer on the inside or the outside

radius; a negative value of n represents a beam which is stiffer on the inside, and a positive value of n represents one which is stiffer on the outside. Tangential heterogeneity can be represented by adjusting the value of k to match the frequency of the fiber waviness.

Finite Element Analysis

A linear finite element model is used to verify the results of the elasticity analysis. The model consists of 300 four node quadratic elements where the properties are input for each element to handle the material heterogeneity. The pure bending boundary conditions are applied by distributing the appropriate normal loads at the nodes along the straight edges. The results are within 8 % of the analytical results from the elasticity analysis.

Results

Stresses in the curved beams are affected by the geometry of the beam as well as the material heterogeneity. Figure 16 shows the relative shape of several beams with different radius to depth ratios, R/t. An R/t ratio of 25 or greater is typical of the curved beams used as primary structures in an aircraft fuselage. Figure 17 shows the effect of radial heterogeneity on the maximum radial stress for several different R/t values. The degree of radial heterogeneity, n, is varied from -2 to 2, where an n value of -2 corresponds to a 20% drop in stiffness from the inside radius to the outside and an n value of +2 corresponds to a 20% increase in stiffness. Figure 17 shows that for a radius to depth ratio of 1.0, the maximum radial stress is affected greatly by the value of n , but for an R/t value greater than 10.0, the degree of radial heterogeneity has no effect on the maximum radial stress. Figure 18 shows similar results for the effect of n on the maximum tangential stress. The degree of tangential heterogeneity, k, was found to have no effect on the stresses in the beam, but does have an effect on the deflection as well as the failure of the beam.

Maximum Stress Failure Analysis

The maximum stress failure criterion is used to compare the performance of beams made with the microstructures shown in Figure 14. The maximum tensile, compressive and shear stresses are determined for the beam and are compared to the corresponding ultimate loads of the material. The maximum moment to failure is determined by increasing the applied moment until one of the stresses exceeds the corresponding ultimate load. The moment to failure is determined for a beam with an inside radius of 3.5 inches, an outside radius of 4.5 inches and an included angle of 90°.

Several different unidirectional microstructures are compared; the first has tangentially oriented fibers, the second is the curved beam cut from a straight unidirectional panel, and the third has curved fibers, but not the same curvature as the beam. Data for this microstructure was taken from a part

produced by diaphragm forming. A beam with patchwork tangentially oriented fibers is also compared to the unidirectional microstructures. Two quasi-isotropic microstructures are also compared, one with axisymmetric fiber orientation as obtained from stretching a straight beam and another which represents a curved pattern cut from a quasi-isotropic panel. The analysis is conducted for an 8-ply lay-up so that the weight of all microstructures is the same. Table 4 compares the moment to failure of the different microstructures as well as the maximum deflection for a unit load. Unidirectional beams with non-tangentially oriented fibers result in considerable reduction of the moment to failure and a considerable increase of the maximum deflection. The two quasi-isotropic microstructures have virtually the same moment to failure and maximum deflection.

Conclusions

This paper briefly outlines a series of analyses that can be used to predict structural performance from basic processing information and material preform design for long discontinuous fiber thermoplastics. This information is important to the material manufacturer and the process designer as well as the structural designer. Although much needs to be added, these tools represent the basis for a truly integrated design methodology for composite structures.

References

1. G. K. Batchelor, "The Stress Generated in a Non-dilute Suspension of Elongated Particles by Pure Straining Motion," Journal of Fluid Mechanics, Vol. 46, part 4, 1971, pp. 813-829.

2. R. L. McCullough, G. J. Jarzebski, S. H. McGee, "Constitutive Relationships for Sheet Molding Materials," The Role of the Polymeric Matrix in the Processing and Structural Properties of Composite Materials," Plenum Press, New York, N. Y., (1983).

3. S.G. Lekhnitskii, Theory of Elasticity of an Anisotropic Body, Mir Publishers, Moscow, 1981

Table 1. Summary of Property Predictions

Term	Newtonian Fluid	Power-Law Fluid
η_{11}/η	$\frac{f}{2}\left[\frac{\sqrt{\bar{f}}}{1-\sqrt{\bar{f}}}\right](L/D)^2$	$2^{-m}f\left[\frac{\sqrt{\bar{f}}}{1-\sqrt{\bar{f}}}\right]^m(L/D)^{m+1}\dot{\varepsilon}_1^{\,m-1}$
η_{12}/η	$\frac{1}{2}\left[\frac{2-\sqrt{\bar{f}}}{1-\sqrt{\bar{f}}}\right]$	$2^{-m}\left[\frac{2-\sqrt{\bar{f}}}{1-\sqrt{\bar{f}}}\right]^m\dot{\gamma}_{12}^{m-1}$
η_{23}/η	$\left[1-\sqrt{\bar{f}}\right]^{-1}$	$\left[1-\sqrt{\bar{f}}\right]^{-m}\dot{\gamma}_{23}^{m-1}$
η_{22}/η	$4\left[1-\sqrt{\bar{f}}\right]^{-1}$	$4\left[1-\sqrt{\bar{f}}\right]^{-m}\dot{\varepsilon}_2^{\,m-1}$
η_{23}/η_{12}	$2\left[2-\sqrt{\bar{f}}\right]^{-1}$	$2^m\left[2-\sqrt{\bar{f}}\right]^{-m}$
η_{11}/η_{22}	$2^{-3}f\,\bar{f}^{\,1/2}(L/D)^2$	$2^{-(m+2)}f\,\bar{f}^{\,m/2}(L/D)^{m+1}$

Table 2. Apparent Laminate Viscosities, Laminate Theory

Laminate	$\bar{\eta}'_{11}/\eta$	$\bar{\eta}'_{22}/\eta$	$\bar{\eta}'_{12}/\eta$	$\bar{\lambda}'_{12}$	$\bar{\lambda}'_{21}$
$[0/90]_s$	1.04×10^{6}	1.04×10^{6}	4.48	1.52×10^{-5}	1.52×10^{-5}
$[0/\pm45]_s$	6.96×10^{5}	2.32×10^{5}	3.48×10^{5}	1.0	3.33×10^{-1}
$[0/\pm45/90]_s$	6.96×10^{5}	6.96×10^{5}	2.61×10^{5}	3.33×10^{-1}	3.33×10^{-1}
$[\pm45]_s$	1.79×10^{1}	1.79×10^{1}	5.22×10^{5}	1.0	1.0

f = 0.6 L/D = 1000

$\eta_{11}/\eta = 2.09\times10^{6}$ $\eta_{22}/\eta = 3.18\times10^{1}$ $\eta_{12}/\eta = 4.48$

$\mu_{11}/\eta = 2.09\times10^{6}$ $\mu_{12}/\eta = 1.59\times10^{1}$ $\mu_{22}/\eta = 3.13\times10^{1}$

$\mu_{66}/\eta = 4.48$

Table 3. Constrained (LPT) and Unconstrained (UCT) Laminate Theory Results

Laminate	$\bar{\eta}'_{11}/\eta$ LPT	$\bar{\eta}'_{11}/\eta$ UCT	$\bar{\eta}'_{22}/\eta$ LPT	$\bar{\eta}'_{22}/\eta$ UCT	$\bar{\eta}'_{12}/\eta$ LPT	$\bar{\eta}'_{12}/\eta$ UCT
$[0/90]_s$	1.04×10^{6}	1.04×10^{6}	1.04×10^{6}	1.04×10^{6}	4.48	4.48
$[0/\pm45]_s$	6.96×10^{5}	6.96×10^{5}	2.32×10^{5}	2.10×10^{1}	3.48×10^{5}	2.26×10^{1}
$[0/\pm45/90]_s$	6.96×10^{5}	5.22×10^{5}	6.96×10^{5}	5.22×10^{5}	2.61×10^{5}	1.81×10^{1}
$[\pm45]_s$	1.79×10^{1}	1.57×10^{1}	1.79×10^{1}	1.57×10^{1}	5.22×10^{5}	3.17×10^{1}

Table 4. Microstructural Comparison of Beams Loaded in Pure Bending

Fiber Orientation	Moment to Failure	Maximum Deflection
Unidirectional Tangential	1.00	1.00
Unidirectional Cut-out	0.39	1.14
Unidirectional Non-tangential	0.46	1.09
Unidirectional Patchwork	0.70	1.36
Quasi-isotropic axisymmetric	1.00	1.00
Quasi-isotropic Cut-out	0.97	1.00

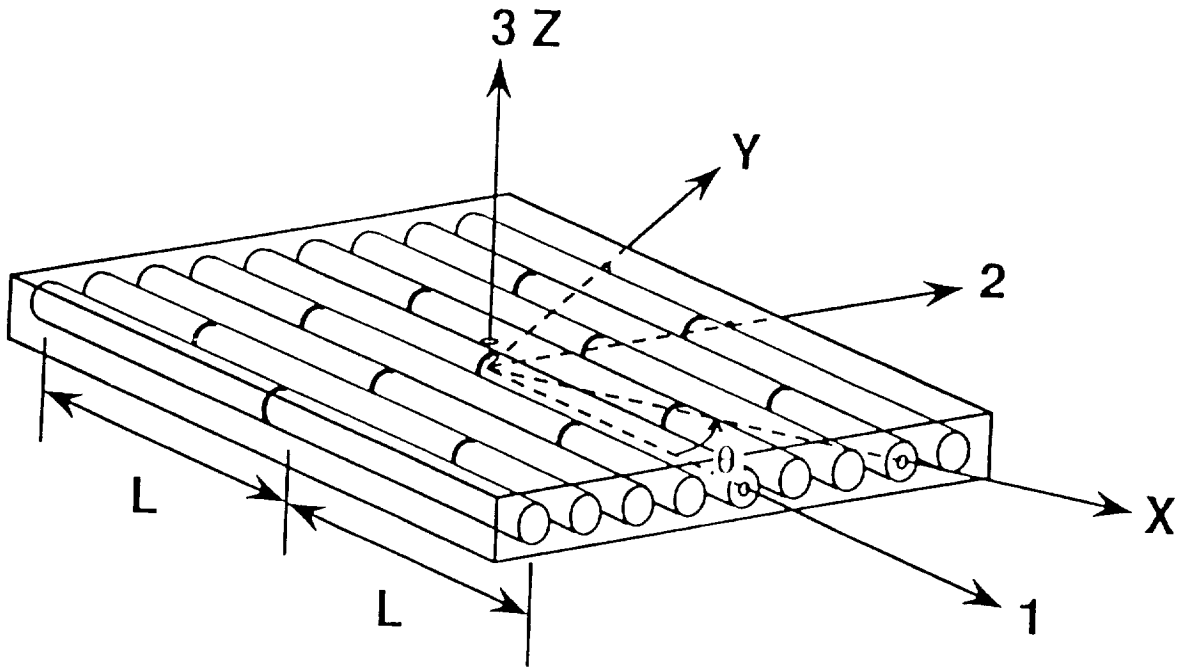

Figure 1. Oriented Fiber Assembly

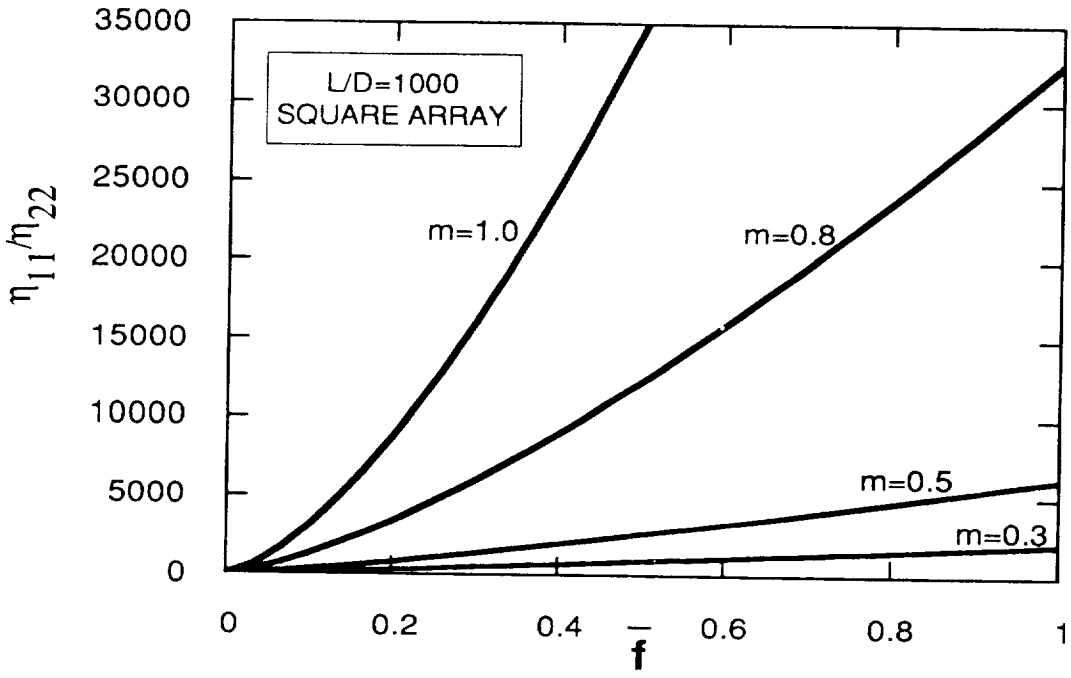

Figure 2. Ratio of Axial and Transverse Elongational Viscosities

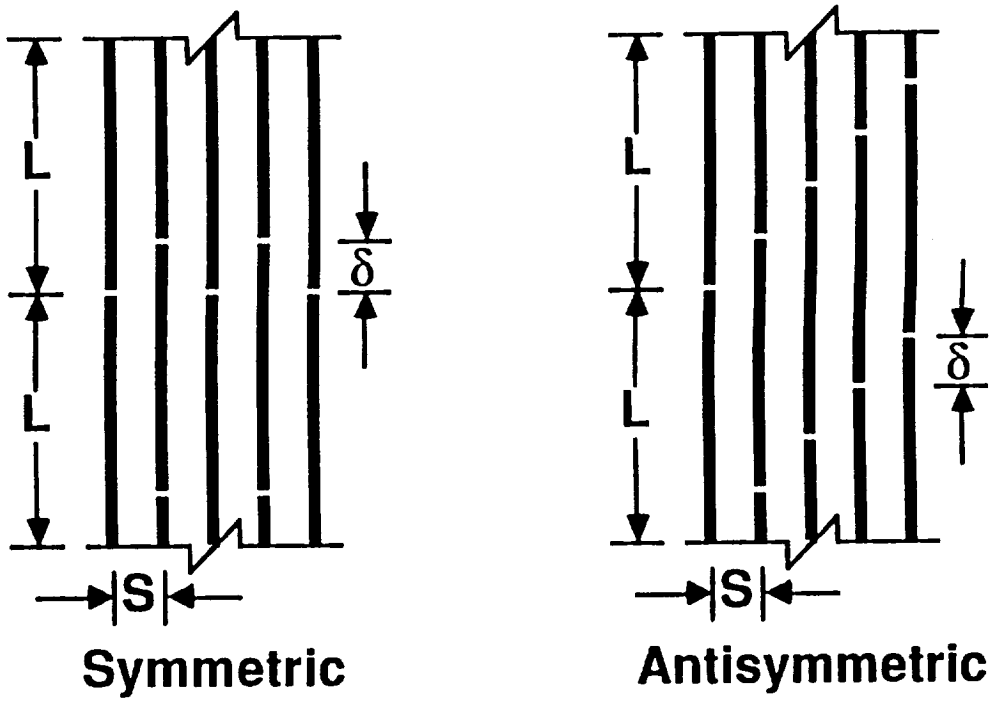

Figure 3. Overlap Length Geometry

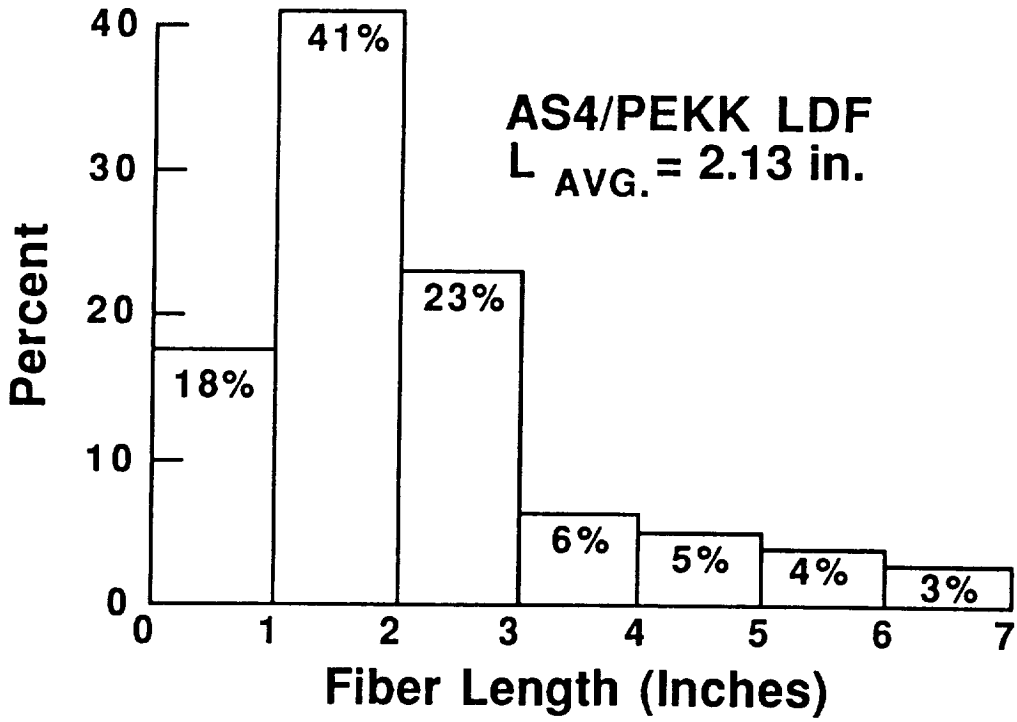

Figure 4. Fiber Length Distribution

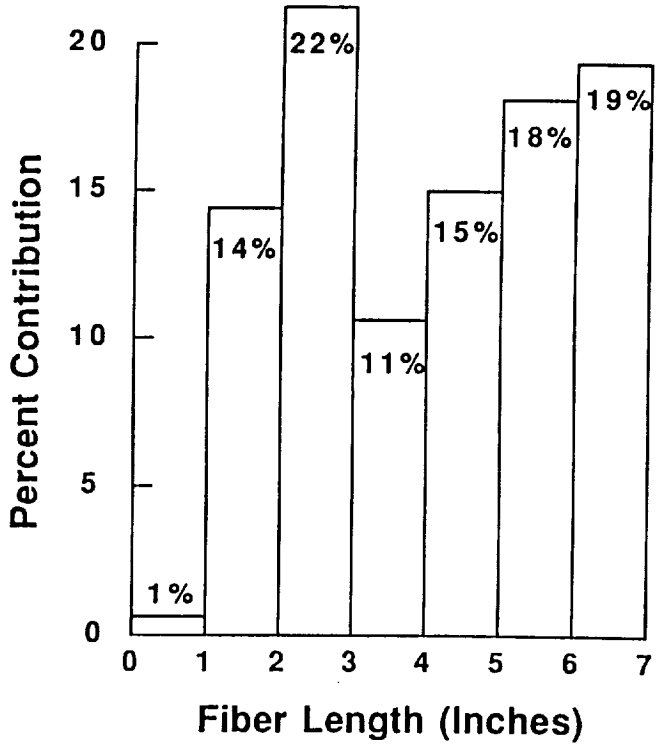

Figure 5. Fiber Length Contribution to Effective Viscosity

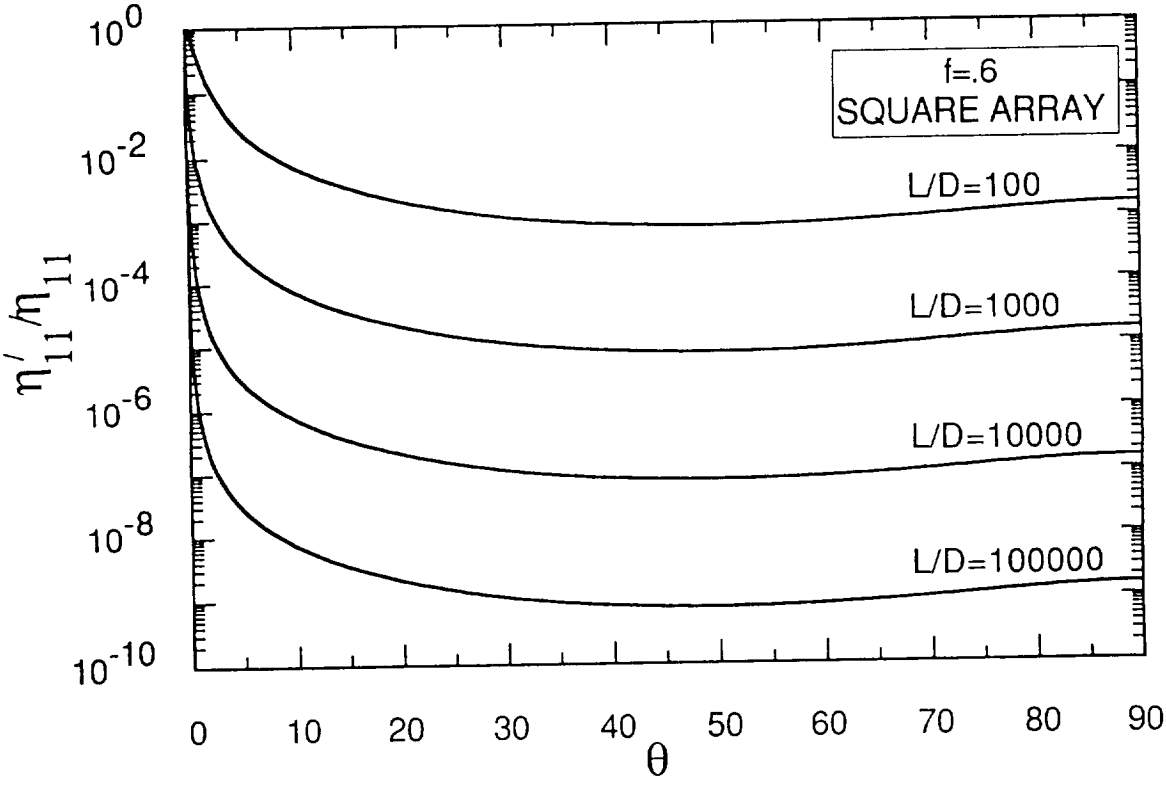

Figure 6. Influence of Fiber Orientation on Elongational Viscosity

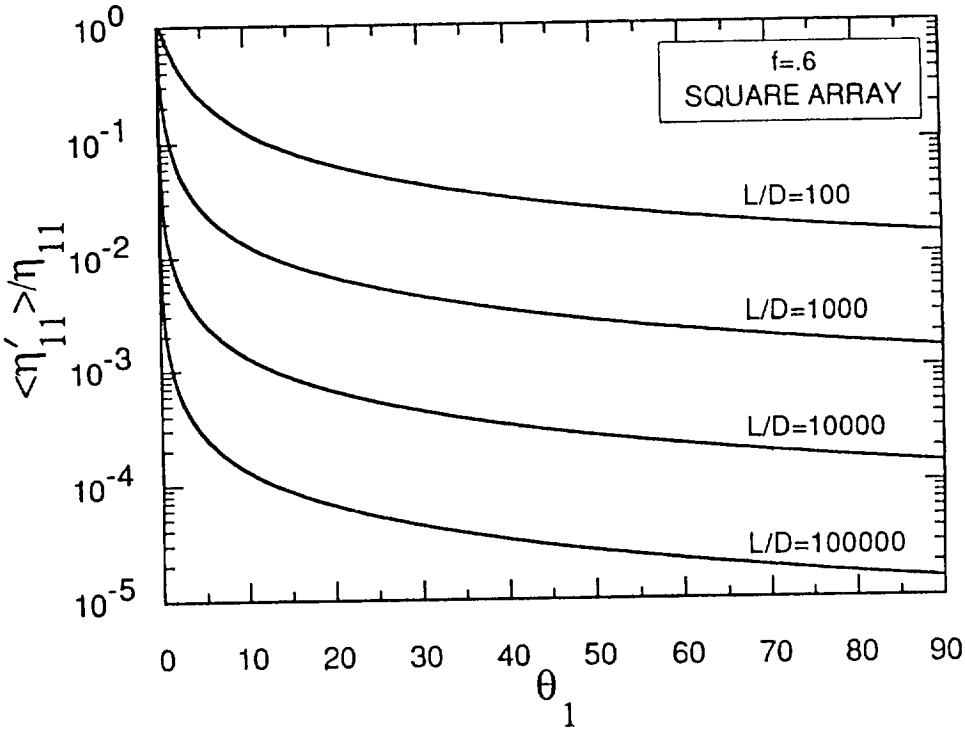

Figure 7. Effect of Orientation Distribution on Elongational Viscosity

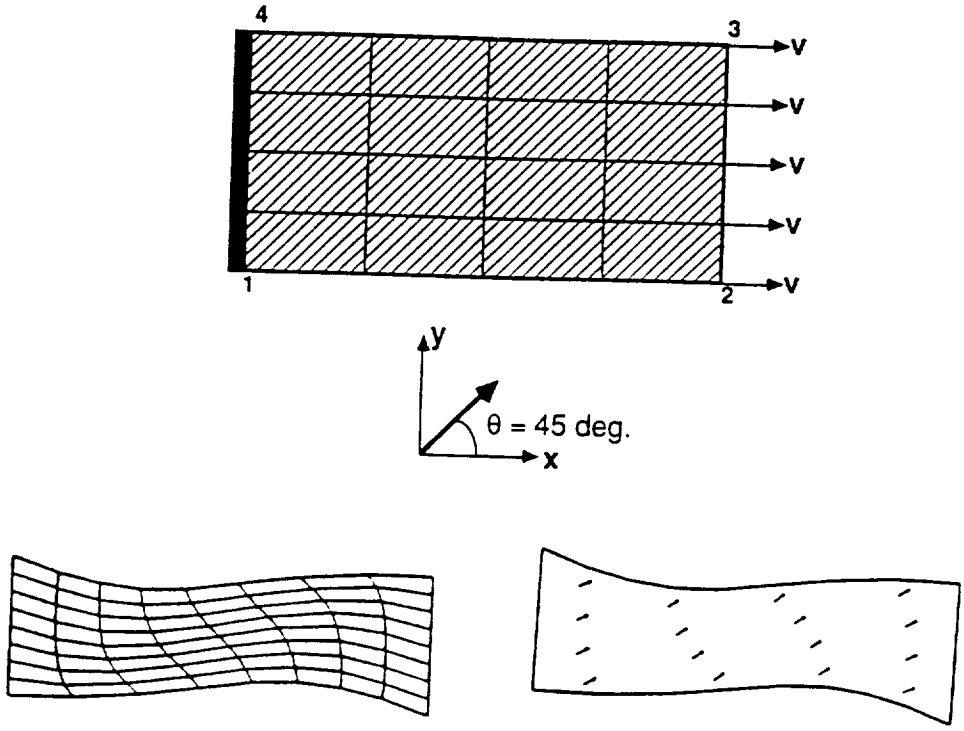

Figure 8. Off Axis Tension Test a) Problem Geometry b) Deformation After 20 Time Steps c) Fiber Orientation After 20 Time Steps

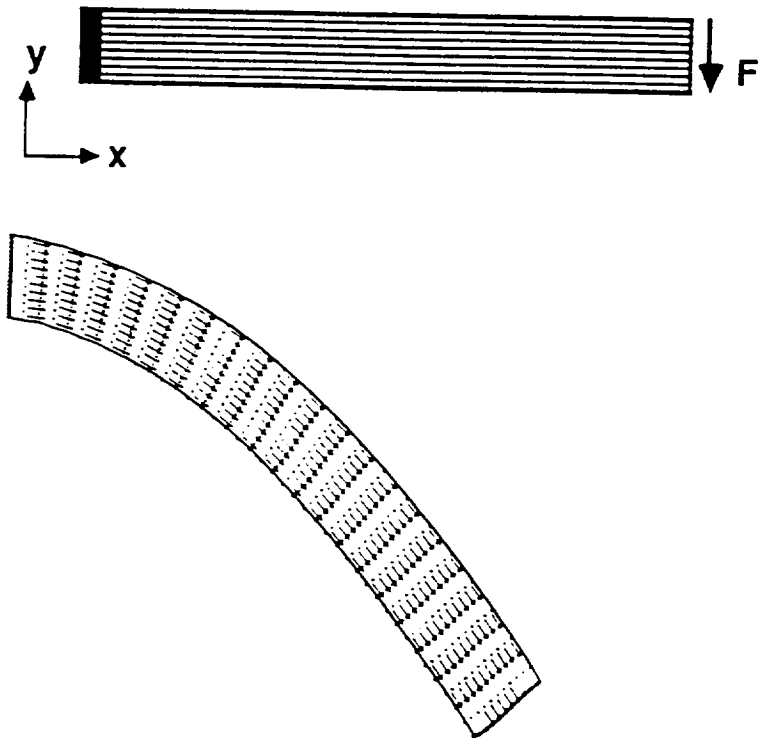

Figure 9. Bending of a Sheet of Unidirectional Material a) Problem Geometry b) Deformed Geometry

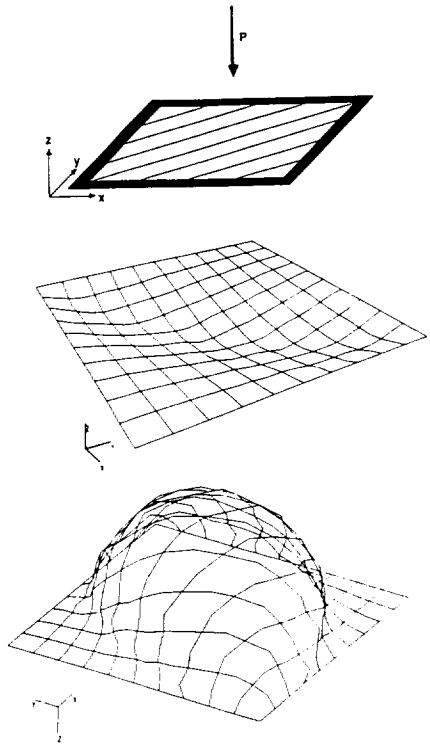

Figure 10. Bulging of a Clamped Sheet a) Problem Geometry b) Deformation After 20 Time Steps c) Deformation After 59 Time Steps

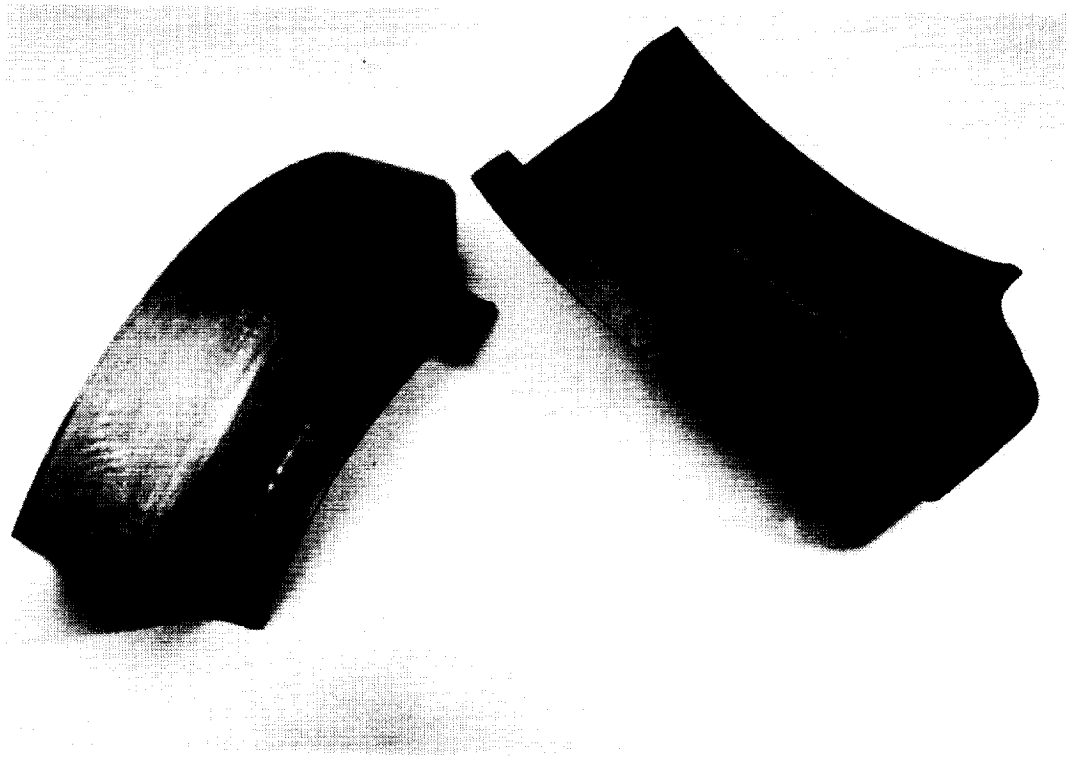

Figure 11. Diaphragm Formed Curved Beams

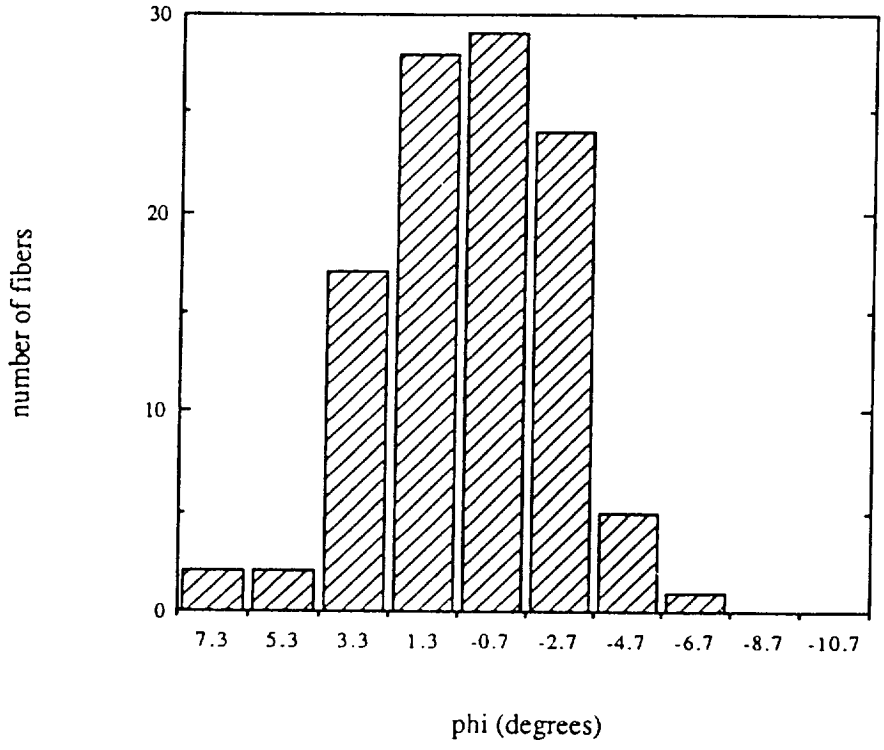

Figure 12. Fiber Orientation Histogram of Processed Material

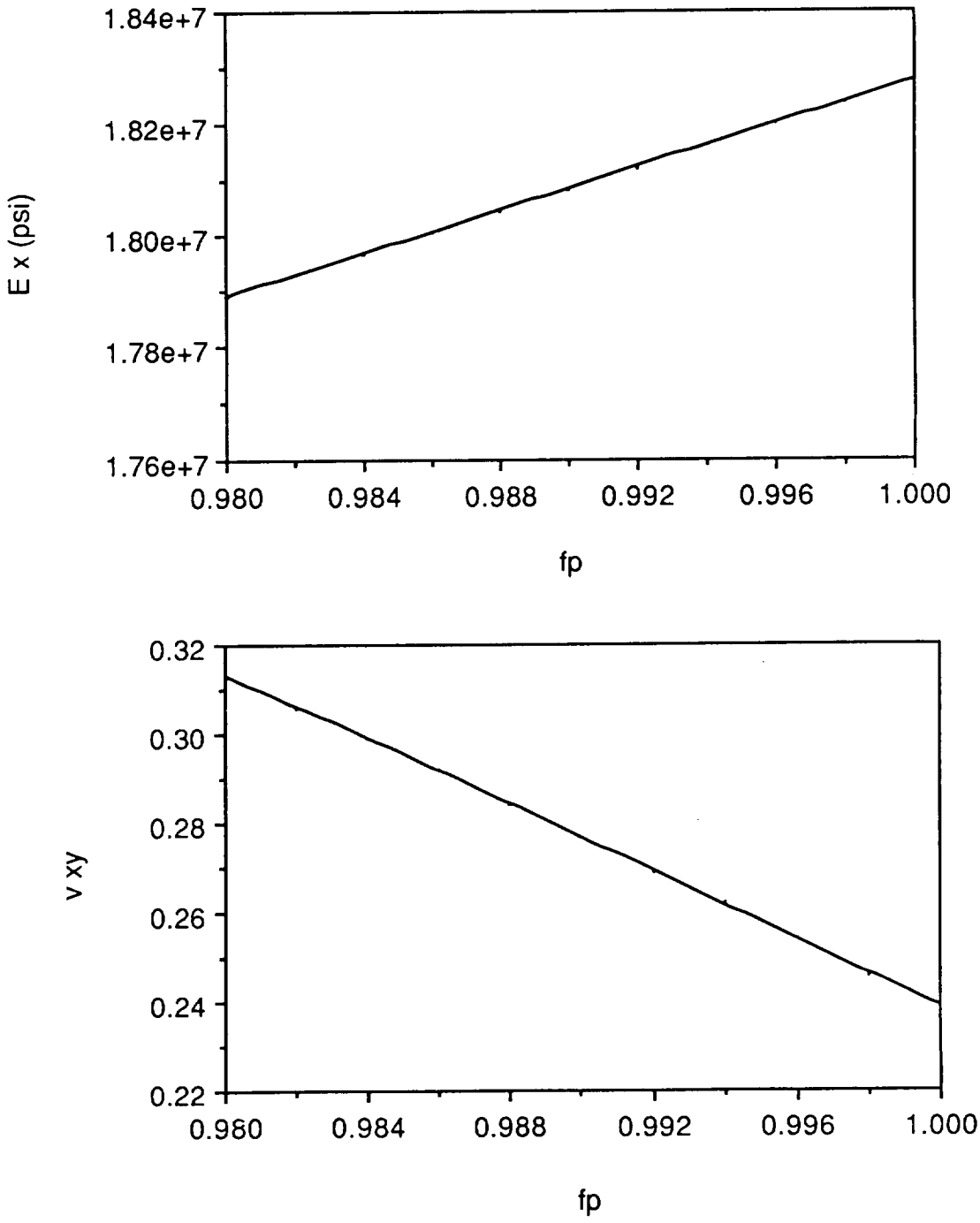

Figure 13. Material Properties vs. Relative Fiber Alignment

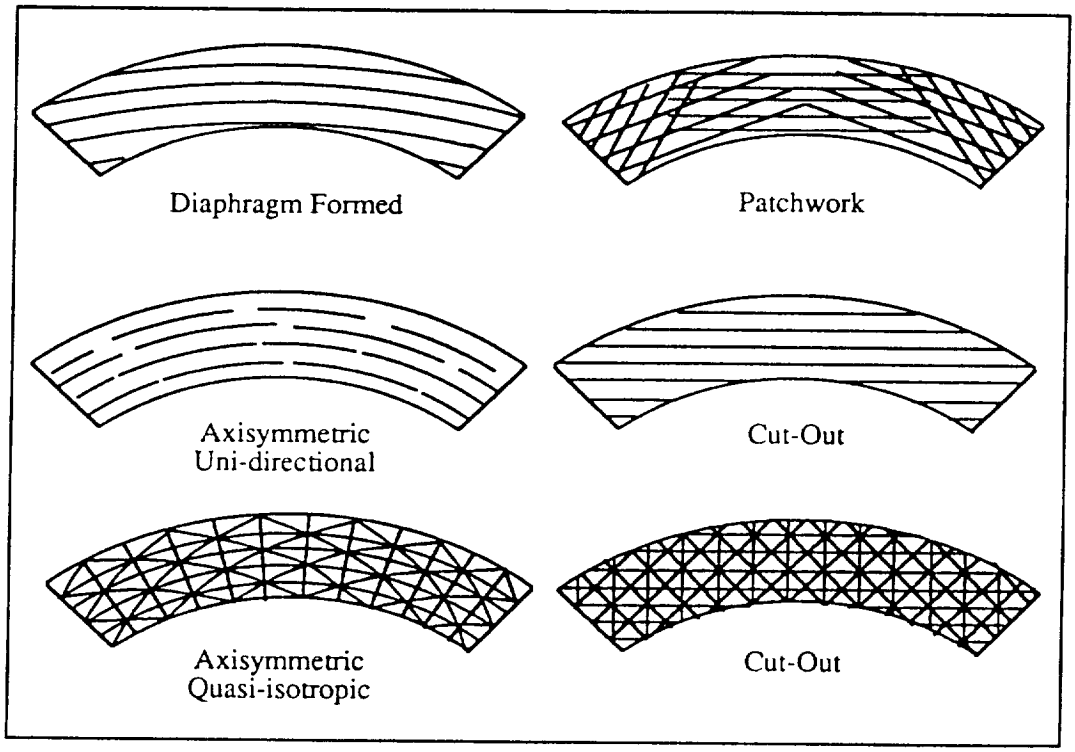

Figure 14. Comparison of Beam Microstructures

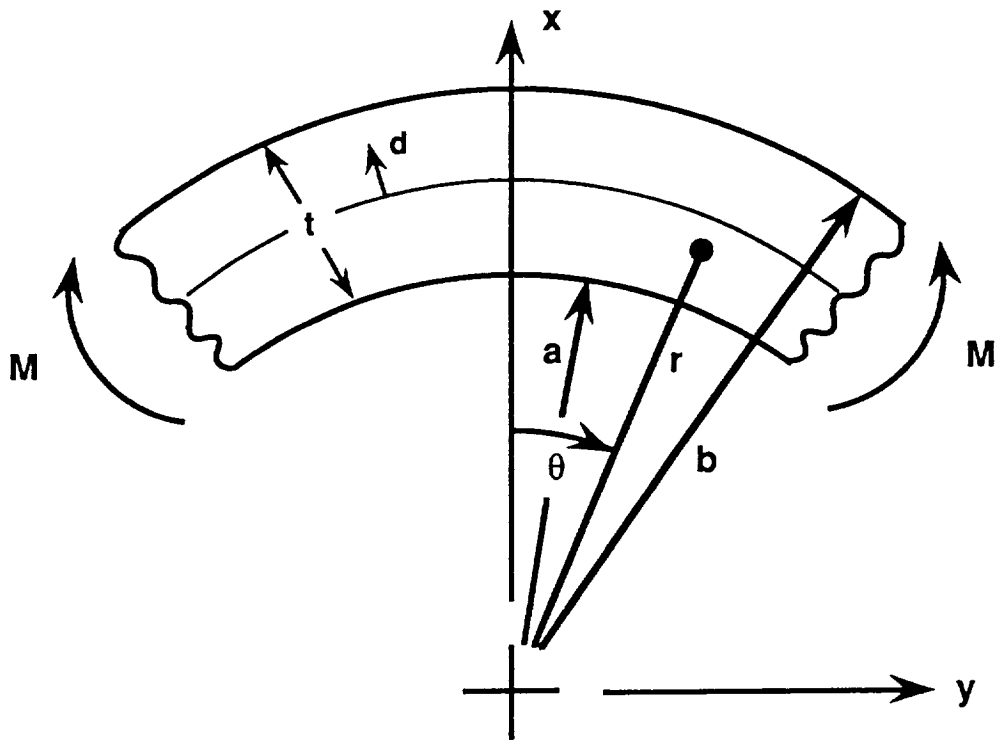

Figure 15. Pure Bending Load Case

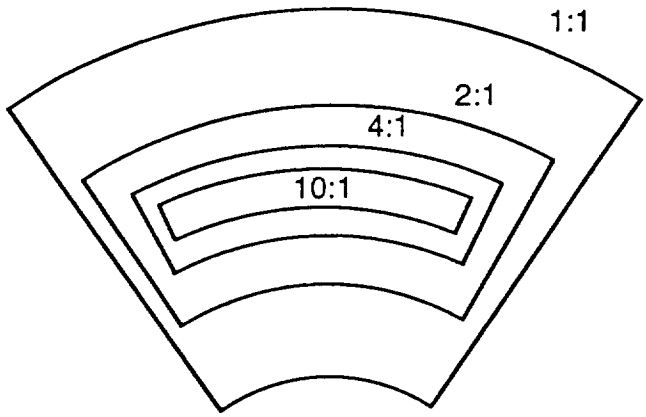

Figure 16. Comparison of Several Different Beam Geometries

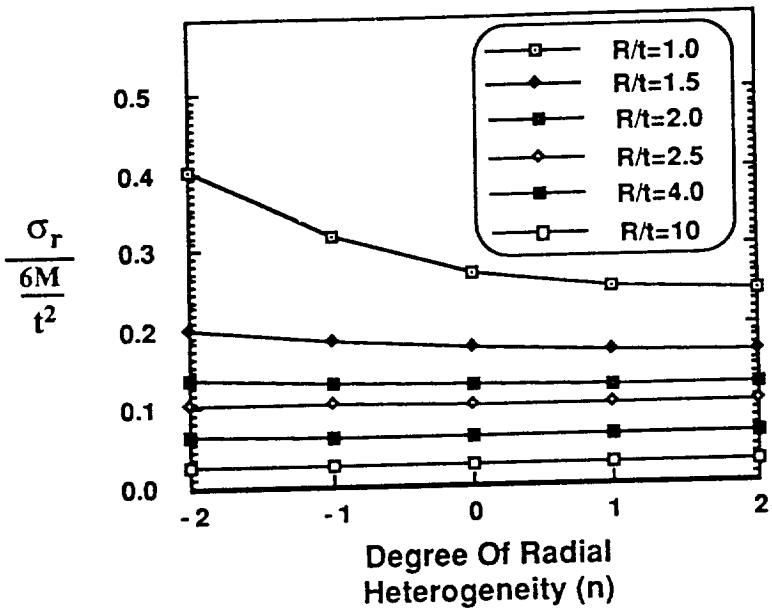

Figure 17. Maximum Radial Stress vs. Degree of Radial Heterogeneity

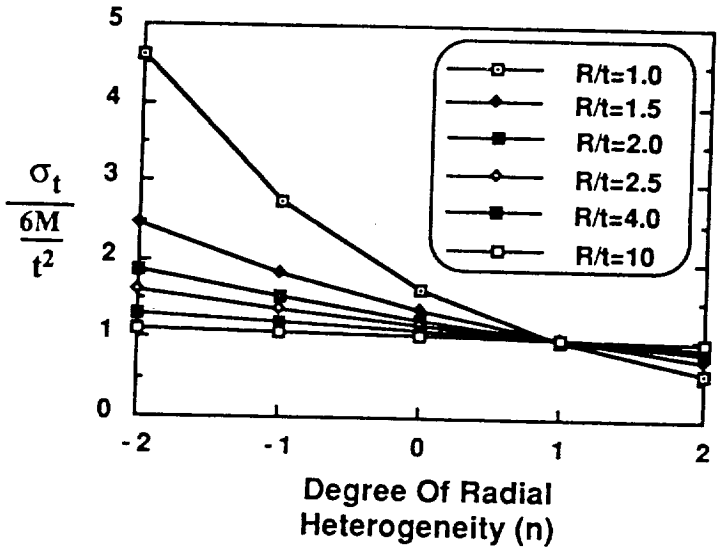

Figure 18. Maximum Tangential Stress vs. Degree of Radial Heterogeneity